Voltage-Gated Hydrophobic Nanopores

Sergei N. Smirnov,[‡,*] Ivan V. Vlassiouk,[†,*] and Nickolay V. Lavrik[§]

[†]Measurement Science & System Engineering Division, Oak Ridge National Laboratory, Oak Ridge, Tennessee 37931, United States, [‡]Department of Chemistry and Biochemistry, New Mexico State University, Las Cruces, New Mexico 88003, United States, and [§]Center for Nanophase Materials Sciences, Oak Ridge National Laboratory, Oak Ridge, Tennessee 37831, United States

ABSTRACT Hydrophobicity is a fundamental property that is responsible for numerous physical and biophysical aspects of molecular interactions in water. Peculiar behavior is expected for water in the vicinity of hydrophobic structures, such as nanopores. Indeed, hydrophobic nanopores can be found in two distinct states, dry and wet, even though the latter is thermodynamically unstable. Transitions between these two states are kinetically hindered in long pores but can be much faster in shorter pores. As it is demonstrated for the first time in this paper, these transitions can be induced by applying a voltage across a membrane with a single hydrophobic nanopore. Such voltage-induced gating in single nanopores can be realized in a reversible manner through electrowetting of inner walls of the nanopores. The resulting *I*—*V* curves of such artificial hydrophobic nanopores mimic biological voltage-gated channels.

KEYWORDS: hydrophobic nanopore · voltage gating · surface conductance

Semiconductor devices are based on controlling the current carried by electrons and holes. Nature, on the other hand, employs ionic and molecular fluxes through phospholipid membranes offering a broader range of mechanisms of control that are selective and responsible for a variety of metabolic and signaling purposes. While natural channels are usually less than a few nanometers in diameter, artificial nanopores can be produced of different dimensions, including much larger diameters and lengths, not only to mimic nature but also to explore new mechanisms of ionic current gating.

Many of these mechanisms have been previously discussed. The most obvious one is physical blockage that happens due to changing of pore dimensions *via* its expansion/shrinkage or by guest molecules captured inside or translocating through the channel.[1−4] Such blockage is difficult to achieve in full for "large" pores and can lead only to some decline in the ionic current through the pore. This decline is proportional to the volume of the molecule(s) that entered the pore, in analogy to operation of a Coulter counter device, hence the volume exclusion mechanism.[4] The surface charge mechanism can offer a more significant gating of ions through large pores if the overall ion concentration is small. As the name states, the charged walls of the pore exclude ions of the same charge, while ions of the opposite charge maintain electroneutrality and their concentration can exceed that of the ions outside the pore.[5] As it was demonstrated experimentally[6−8] and theoretically,[9,10] this mechanism can be employed for gating current of both ions simultaneously when the pore walls have nonuniform charge distribution. For example, if a nanopore has two halves with oppositely charged walls, the resulting diode would carry ionic current in the open state greater than that if the walls were neutral. At the same time, the ionic current through such a diode would drop to a much smaller current in the closed state with the opposite bias. The resulting rectification factor, the ratio between the open and closed state currents, can exceed 200.[6]

The third mechanism is based on hydrophobicity switching and has a much more dramatic gating effect that can exceed 6 orders of magnitude in the ionic current variation;[11−13] it affects not only ions but also the overall solution flow through the nanopore. The mechanism involves hydrophobic nanopores that are impermeable to water intrusion but can be switched off (and on) in response to physical or chemical stimuli.[11−15] The latter requires engineering of mixed monolayers that have both hydrophobic molecules and sensor molecules making surfaces sensitive to pH,[14] light,[11] or bioanalytes.[15] The pores with large diameter (>20 nm) do not expel water (dewet) even after the surface hydrophobicity is restored. In such pores, despite a greater thermodynamic stability of the dry state with water expelled from the pore, the wetted state is kinetically stalled because of a high activation barrier for dewetting.[13,16−21]

* Address correspondence to snsm@nmsu.edu, vlassioukiv@ornl.gov.

Received for review June 28, 2011 and accepted August 14, 2011.

Published online August 15, 2011
10.1021/nn202392d

Hydrophobicity is a fundamental property that is responsible for numerous physical and biophysical aspects of the behavior of nonpolar substances in water. A strong attraction between water molecules, coming from their hydrogen bonding, makes the interaction between water and nonpolar molecules unfavorable and causes water restructuring near hydrophobic surfaces.[21] The interplay between hydrophobic and hydrophilic properties is responsible for conformational changes in biologically important molecules and their biochemical functionality. For example, biological membranes with their hydrophobic interior are impermeable to most ions (and many hydrophilic molecules) and rely on the membrane channels that control their transport. The channels employ a variety of mechanisms for efficient and often selective transport of molecules and ions across cell membranes, which is imperative in a large variety of metabolic and signaling purposes, *i.e.*, in sustainable life of organisms. For example, the transmission of nerve impulses depends upon ionic currents generated by the controlled release of ions across membranes. Some ionic channels in the cell membrane are believed to employ the variations between hydrophobic and hydrophilic states that are gated for water and ion flow either by bias or by analytes.[22−27] Understanding these mechanisms is important for comprehension of cell functioning; designing of artificial nanochannels with adaptable hydrophobicity should elucidate the mechanism of the hydrophobicity switching phenomenon.

Here we describe an investigation of ionic conductance in short artificial hydrophobic nanopores and demonstrate that they can be switched from the dry nonconductive to the wet conductive state by means of applying large enough potential. Our goal is to elucidate this voltage gating mechanism for pores larger than the typical size of membrane channels but short enough for voltage gating realization. In contrast to long nanopores of similar diameters, the conductive state attained in such short hydrophobic nanopores can be made to either retain or retreat with changing bias. A possibility of such control offers new applications in nanopore-based nonlinear elements.

RESULTS AND DISCUSSION

Hydrophobic surfaces are characterized by a contact angle with water, θ_a, greater than 90°, as is identified by the Young equation relating the surface tension difference, $\Delta\gamma$, between the wall/vapor, γ_{wv}, and wall/liquid, γ_{wl}, interfaces to that of the free liquid/vapor interface, γ:

$$\Delta\gamma = \gamma_{wv} - \gamma_{wl} = \gamma \cos\theta_a \qquad (1)$$

A hydrophobic nanopore remains dry until the external pressure exceeds the critical value, ΔP_o, which depends on $\Delta\gamma$ (*i.e.*, on the surface modification) and the pore diameter, D:

$$\Delta P_o = -\frac{4\gamma \cos\theta_a}{D} \qquad (2)$$

The subscript in θ_a emphasizes that it is a maximum (or critical) advancing angle that a droplet can sustain without moving, which often is noticeably greater than the (minimum) receding angle, θ_r. Because of this hysteresis and a changing shape of the nanopore entrance, the actual angle of the water meniscus can accept any value in between and changes in response to the altered pressure difference. Upon reaching the critical pressure for intrusion, ΔP_o, the contact angle exceeds the critical one, θ_a. The value of ΔP_o is quite large; even for D = 300 nm and hydrophobic modification with a modest advancing contact angle of $\theta_a \approx$ 100°, its value is ΔP_o > 1.6 bar.[12] For an electrolyte, instead of just water, its intrusion into the nanopore would cause electrical shorting measurable by a drastic drop in resistance,[13] which, as we describe below, in short nanopores can be induced by an increased bias.

Figure 1 illustrates typical current voltage characteristics for two nanopores with similar diameters (120 and 140 nm), the surface of which was hydrophobically modified by SiH_{16}. At low bias sweeps (±0.1 V in Figure 1A and C), the pores are dry and show very low conductance, corresponding to the trace labeled I in the figure. Increasing the sweep eventually electrically shorts the pores (1B and 1D) at a high enough critical bias, $U_c \approx$ 4 V in 1B and $U_c \approx$ 1 V in 1D. The conductance recovers to almost zero when the bias is lowered, and the procedure can be repeated. If the highest bias value is further increased, the low bias conductance upon return starts showing a partial residual shorting seen as hysteresis in 1B (and trace III), which often leads to recovery of the closed dry state after some time. Further bias increase may result in "complete shorting" (trace IV), the conductance in which coincides with that of the unmodified pore.

Comparing Figure 1B and D reveals significant variability in the current voltage behavior. The nanopore having a diameter of 120 nm (Figure 1D) exhibits almost no hysteresis in a broad range of biases (up to ±3 V), in contrast to what is seen for a 140 nm pore with the same modification (Figure 1B). The critical bias for shorting is also noticeably smaller, $U_c \approx$ 1 V for 1D instead of $U_c \approx$ 4 V for 1B. One can see that there is much greater noise near the critical bias (see Figure 2), which makes it also difficult to define the value of critical bias precisely.

The possible mechanisms of the observed electrical gating can be divided into two kinds, sketched in Figure 3. The first kind does not involve movement of the three-phase contact line along the nanopore wall. Instead, bending of menisci induced by attractive electrostatic forces causes the two water−vapor interfaces to overlap. At high enough electric field, bending

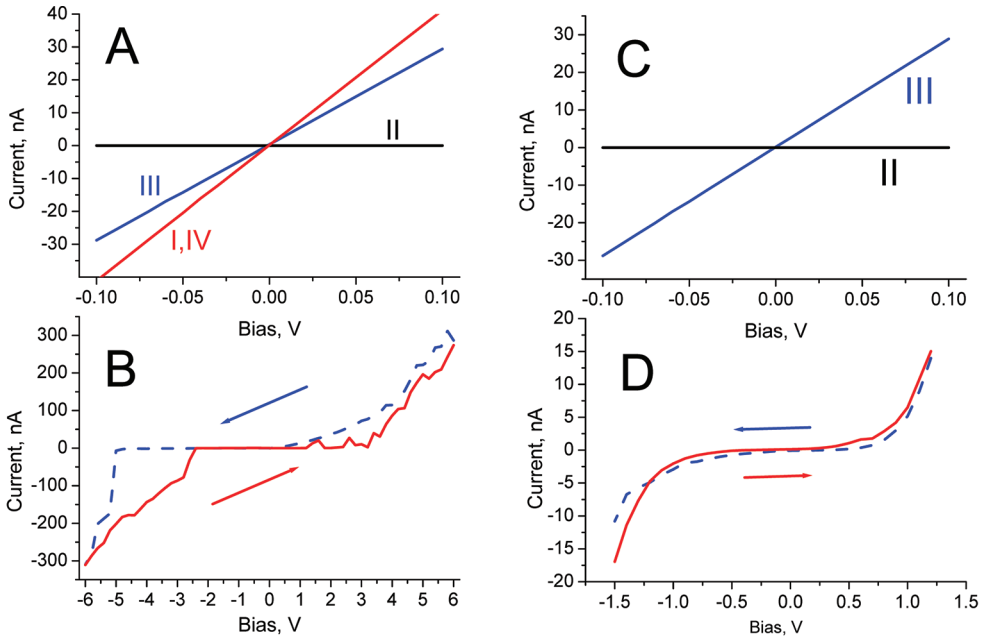

Figure 1. Typical examples of voltage-induced gating in hydrophobic nanopores with 140 nm diameter (A and B) and 120 nm (C and D) modified with SiH_{16}. (A) Before hydrophobic modification the pore is hydrophilic and shows conductance in agreement with its size (I). After modification, the pore is dry despite being in electrolyte (1 M KCl in Tris buffer) and shows a very low conductance at low bias sweeps (II). Increasing the sweep eventually electrically shorts the pore (B) at a high enough bias ($U_c \approx 4$ V in the figure). The conductance recovers to almost zero when the bias is decreased (with a noticeable hysteresis), but with further increase of the sweep it may end up shorted to a partial extent (III) or in full (IV). The latter usually occurs at much larger bias sweeps. The second nanopore (C and D) demonstrates a similar behavior but with significantly smaller critical voltage for shorting ($U_c \approx 1$ V) that correlates with a measurable conductance in the closed state.

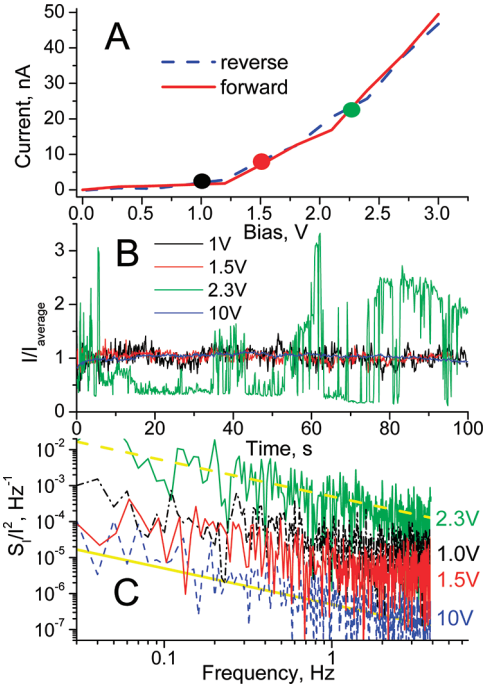

Figure 2. (A) Nanopore with 120 nm diameter modified with SiH_{16} shows a low hysteresis and low shorting critical bias. The current fluctuation is the highest near the transition bias, as indicated by the green trace in B at 2.3 V. (C) Corresponding normalized current power spectral densities, S_I/I^2, for the same biases; the yellow lines depict $1/f$ white noise dependences.

can go beyond just changing the menisci curvature but elongate them analogously to Taylor cone formation at the capillary end in the electrospraying process.[28,29] The second kind involves inward movement of the contact lines due to the exerted electrostatic pressure accompanied by changes in the critical contact angle when the voltage across the nanopore is applied. The contact angle change phenomenon is associated with electrowetting. In both kinds, the critical voltage that induces wetting of the initially dry nanopore should depend on the pore dimensions. The primary difference is that the type of hydrophobic surface modification is more decisive for the second kind and is of little importance in the first one.

For a negligible conductance through the membrane and the pore walls, an almost linear drop of the applied bias through the gap induces electrostatic attraction of the opposite water menisci and causes them to bend toward each other (see Figure 3B). Because of such bending, it also increases the contact angle at the water/wall surface. The overlap without movement of spherical menisci can occur only when the pore diameter is greater than the pore length, H, even if the contact angle is $\theta_a = 180°$. Since the critical contact angles are smaller than 180°, such an overlap can be realized without moving the contact line only when the ratio D/H is significantly greater than 1. Having a large D/H ratio is not desirable, as there would

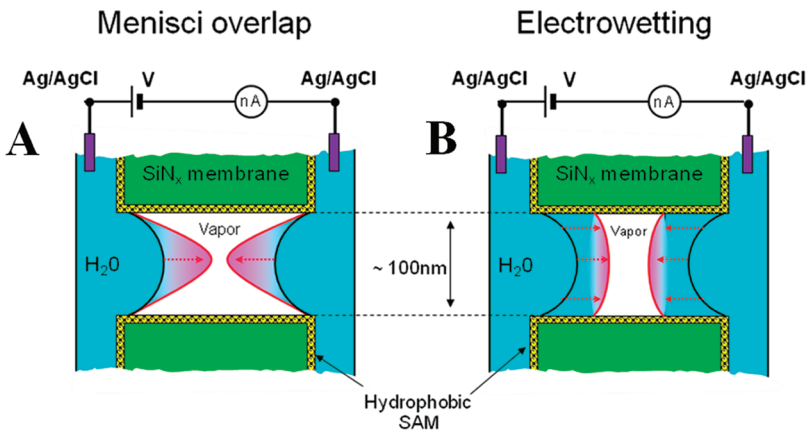

Figure 3. Illustration of the two possible mechanisms for voltage-induced water intrusion into a hydrophobic nanopore. (A) The left side corresponds to no movement of the contact line, when electrostatic pressure can only bend the menisci until contact. (B) The case on the right depicts electrowetting initiated by decreasing contact angle due to nonzero surface conductance producing significant voltage drop at the contact line, which moves the contact lines of both menisci by electrostatic pressure until contact. The menisci can further bend or develop electrospinning jets in the last stages for cases when the electrowetting-induced change of the contact angle is not significant and the contact lines move slowly.

be no thermodynamic advantage for pore dewetting: the surface area of a cylinder becomes smaller than the surface area of two hemispheres for $D/H > 1$. This critical ratio is actually smaller due to a smaller surface energy of the water/solid interface than that of water/vapor. Indeed, we experimentally confirmed that devices with a large aspect ratio, $D/H > 1.5$, are nonfunctional: they immediately were shorted even with the modest pressure gradients (<1 atm) used in filling up the devices. Devices with $D/H \approx 1$ do appear dry and closed at first but never recover the dry state after having been once electrically shorted (opened). The length of the nanopores in our experiments was kept at $H = 300$ nm because thinner SiN films frequently showed breakdown at voltages above 2 V, as was verified before milling the pores.

The shape of menisci can actually be different from spherical. It is well known that electrified liquids can experience electrohydrodynamic instability under high electric fields and produce a thin jet of liquid above the threshold field defined by the surface tension, γ, and the droplet diameter, D. The droplet deforms into the Taylor cone with half angle $\theta_T \approx 24.7°$.[28,29] The effect is often referred to as electrospinning or electrospraying. In the limit of $H \gg D$ the corresponding critical bias can be estimated:[28]

$$U_{c,T} \approx 2H\sqrt{\frac{\gamma \cos \theta_T}{\varepsilon_o D}} \qquad (3)$$

Here ε_o is the permittivity of free space. For the typical dimensions used in this study, $D = 150$ nm and $H = 300$ nm, this estimate is quite large, $U_{c,T} \approx 140$ V. Considering an explicit solution for modest H/D would decrease $U_{c,T}$ but not significantly to agree with that experimentally observed. Moreover, eq 3 does not explain the sensitivity to the surface modification that is very pronounced. The critical value U_c increases with increasing the contact angle with water; that is, more hydrophobic fluorinated modifications lead to much larger U_c (Supporting Information) often beyond the stability of a 300 nm thick SiN membrane, ~30 V.

As assigned to the second kind, the electrical shorting can also occur as a result of the contact line movement. When menisci are bent by electrostatic interaction, the contact angle at the interface changes and can exceed the critical value θ_a to allow water intrusion similar to that induced by pressure, as described by eq 2. The exerted electrostatic pressure, P_{el}, arises from the electrostatic energy, $C_m U^2/2$, of a capacitor made of the two water menisci, changing with the gap between them. The latter, at least in the beginning, is close to the membrane thickness, H, leading to an estimate for the capacitance per area of the nanopore as $C_m \approx \varepsilon_o/H$, giving the pressure estimate:

$$P_{el} = -\frac{\partial C_m}{\partial H}\frac{U^2}{2} = \frac{\varepsilon_o}{H^2}\frac{U^2}{2} \qquad (4)$$

which, under the assumption $P_{el} \approx \Delta P_o$, leads to the estimated critical bias for water intrusion:

$$U_{c,P} \approx 2H\sqrt{\frac{2\gamma|\cos \theta_a|}{\varepsilon_o D}} \qquad (5)$$

According to eq 5, the critical value of $U_{c,P}$ increases with the (critical) contact angle, which qualitatively agrees with the larger U_c observed using much more hydrophobic fluorinated modifications. Nevertheless, the $U_{c,P}$ estimated from eq 5 is quite large, ~80 V, even with a modest $\theta_a \approx 100°$ on aliphatic surfaces and the typical dimensions used in this study, $D = 150$ nm, $H = 300$ nm. Equation 5 appears similar to eq 3, and the lower estimate we get this time is due to a smaller $|\cos \theta_a|$. Similarly, a more thorough analysis without assumption of $H \gg D$ would decrease $U_{c,P}$ but still not

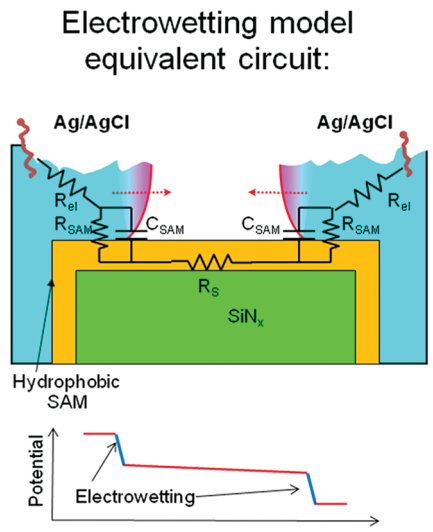

Figure 4. Detailed illustration of the electrowetting model with its equivalent circuit. Charging the capacitance, C_{SAM}, of the hydrophobic monolayer at the contact lines can proceed only if the surface resistance under the layer, R_s, is not very large. Then majority of the applied potential drops at the contact lines and reduces the critical contact angle due to electrowetting.

to the range of that experimentally observed. Another approximation above, $P_{el} \approx \Delta P_o$, also unfavorably increases $U_{c,P}$ in eq 5. The approximation presumes that the initial hydrostatic pressure inside the pore is the same as outside, but we have eliminated all dissolved gases from the solution and from the cell by degassing and thus made the nanopore filled only with water vapor. The outside liquid is at atmospheric pressure and produces an additional (nonelectrostatic) gradient slightly less than 1 atm and thus should further lower the threshold bias. Nevertheless, there is no good correlation of the experimental U_c values with the pore diameter (see Supporting Information), as eq 5 would suggest. Thus the electrostatic pressure mechanism, though showing better qualitative correlation with the experiment, still cannot explain the electrical shorting in full.

A better fit to the experimental data can be found when surface electrowetting is taken into account. This mechanism requires a nonzero conductance along the hydrophobic monolayer. As we have demonstrated before with alumina nanoporous membranes, their surface modification with hydrophobic silanes (similar to those used in this study) prevents water intrusion, but the ionic conductance along the surface is nonzero and depends on the type and the quality of the surface modification.[12,13] The values of such surface resistance are generally very large ($R_s > 10^9$ Ω per square), but its existence significantly alters the charge distribution. Lower R_s causes a greater portion of the voltage drop at the contact lines across the hydrophobic layer (see Figure 4). This permits conditions when electrowetting can alter the surface energy, significantly decreasing the contact angle for the electrostatic pressure to work or even decrease θ_a below 90°. In electrowetting, the contact angle between an electrolyte and a dielectric of thickness d with dielectric constant ε_d separating it from a conductor underneath can be decreased by applying a potential, U, between them. The resulting change of the surface energy due to this electrostatic interaction decreases the contact angle:

$$\Delta(\cos\theta) = \frac{\varepsilon_0\varepsilon_d}{2d\gamma}U^2 \qquad (6)$$

The voltage across the monolayer necessary for the contact angle to drop below 90° can be estimated as

$$U_{c,E} \approx \sqrt{\frac{2d\gamma|\cos\theta_a|}{\varepsilon_0\varepsilon_d}} \qquad (7)$$

For the SiH_{16} modifier with a monolayer thickness of $d \approx$ 1.6 nm and $\varepsilon_d \approx 2.0$, eq 7 suggests that the initial contact angle of $\theta_a = 100°$ can be lowered to less than 90° under a very small voltage drop across the monolayer, $U_{c,E} \approx$ 1.5 V. Actually, there is no need for θ_a to drop below 90°, just lowering it enough eases the way for electrostatic pressure to work. A monolayer that is not perfectly dense has a lower effective thickness and more leakage, thus a lower $U_{c,E}$. Note that the critical bias $U_{c,E}$ depends on the contact angle similar to that of eq 5. It agrees with the above-mentioned higher values of the critical bias for fluorinated surfaces (see Supporting Information), where θ_a is higher than 110°. Similarly, the devices that were treated by a single cycle of SiH_{16} silanization have generally lower critical bias voltages as well. However, repeating silanization, which eliminates imperfections left during the first step, results in an increasing contact angle with water, θ_a, and higher critical biases. The typical values on the SiN side of the chip after the first silanization are within θ_a = 95−100°, while after the second they increase to θ_a = 100−105°. The second silanization improves the packing density of molecules in the monolayer (and thus slightly its thickness) and decreases its effective dielectric constant (due to blocking an ion leakage[30,31]), *i.e.*, increases the electrical capacitance of a monolayer and thus decreases $U_{c,E}$ in eq 7. More importantly, denser packing decreases the electrical conductance along the surface, as described below.

Obviously only a portion of the bias applied to the pore drops across the monolayer near the contact line; the extent of that drop should correlate with the pore resistance in the closed state, R_s (see Figure 4). Equation 7 does not have an explicit dependence on R_s, but it implies that a low conductance along the surface and hence a smaller portion of the voltage drop across the monolayer at the contact line raises the critical voltage. Figure 5 demonstrates this correlation for nanopores modified with SiH_{16}. Some nanopores are represented by connected multiple identical points obtained in

repeated cycles of electrowetting and drying. Such repeated cycling usually (but not always) results in deterioration of the quality of surface modification, as is seen in Figure 5 by randomness of the lines connecting the identical symbols. The empty and filled symbols correspond to devices with a single and double silanization, respectively. The former usually demonstrate higher initial conductances and lower critical bias voltages.

It follows that electrical shorting in hydrophobic nanopores with the dimensions and surface modification employed in this study can be explained as initiated through a combination of electrostatic pressure and electrowetting at the contact line. When the contact angle is decreased by electrowetting to a sufficiently low value, which is still greater than 90°, electrostatic pressure becomes sufficient to pull water inside. At the later stage, when the distance between water menisci noticeably decreases, they can bend enough to overlap. Even though it appears as a very complex process, all mechanisms contribute at different stages, including the menisci bending, without which the electrical shorting would be unable to recover the dry state at low bias, *i.e.*, dewetting.

It is important to note that, similar to what was observed in long hydrophobic nanopores,[13] dewetting of short hydrophobic pores can be favorable thermodynamically but not necessarily kinetically. The thermodynamic advantage of the dry state is very high in long nanopores but decreases with increasing the aspect ratio, D/H, to the extent of it diminishing at $D/H > 1$, as is corroborated by lack of dewetting in pores with $D \approx 300$ nm. A kinetic barrier for dewetting in nanopores with large H/D ratio is defined by a large penalty $\sim\gamma D^2$ for forming a vapor bubble.[17,18] For example, even for a very small diameter $D \approx 15$ nm, this barrier exceeds 1500 kT and makes spontaneous dewetting practically impossible. Our short nanopores, when filled with water by prewetting with alcohol and its gradual change to water, also remain wet at low biases, but electrowetting can produce different outcomes. If the shorting bias does not exceed the critical one significantly, the conductance of such wetted pores upon returning to low biases is only a portion of what it is in a totally wetted state. This partially wetted state quickly recovers to a closed dry state. Applying a bias voltage much greater than the critical one can fill up the nanopore with water completely and render it unrecoverable to the dry state. Of course, a physical removal of water and drying the pore recovers its original hydrophobic state.

So, why is there such a complex behavior with applied bias? The key is the interplay of the two mechanisms. If electrowetting decreases the contact angle well below 90°, the flat menisci collapse without any bubble and thus prevent dewetting due to a large activation barrier. Smaller activation barriers can be

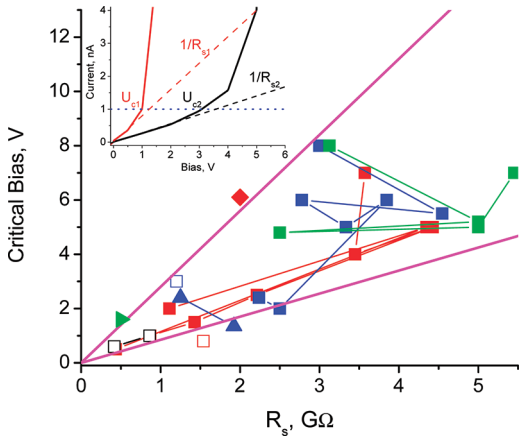

Figure 5. Correlation of the critical bias voltage with the pore resistance in the closed state, R_s. All pores were modified with hexadecylsilane (SiH_{16}). Some pores are represented by multiple points obtained during repeated cycles of wetting and drying. The inset illustrates how the resistance in the closed state and the critical bias voltage, U_c, were identified from the $I-V$ curves on two representative examples.

realized when the menisci "slowly" move toward each other, with the contact angles greater than 90°, under the electrostatic pressure and eventually overlap (electrically short) with a belt-shaped bubble remaining as sketched in Figure 6. At the last stages before their contact, the menisci can further bend to electrospinning jets due to their slow moving contact lines. The existence of this bubble not only makes the ionic conductance smaller than for a fully filled pore but also precipitously reduces the activation barrier for easy dewetting.

The existence of that barrier is the cause of the hysteresis in $I-V$ curves, especially for the pores with large U_c, as in Figure 1B (see also Supporting Information). When the recovery of the closed state proceeds abruptly, it happens at the bias lower than is necessary for initial shorting. The higher the bias used (beyond U_c) to partially open the pore, the closer the resistance to the totally open pore and the longer it takes to recover the closed state. In fact, it can take half an hour if the shorted state has resistance almost equal to that of the totally opened pore (Figure S8, Supporting Information). The same figure illustrates that the contrast in conductance between the on and off states is close to 3 orders of magnitude.

In nanopores with small U_c, where the barrier is small, transitions between the two states can be recognized by a large noise at biases in the vicinity of U_c, where the barrier is even lower (Figure 2B). The normalized current power spectral density, S_I/I^2, is the lowest for high biases, when the pore is totally opened (10 V in Figure 2C). At low frequencies, the noise appears to follow Hooge's relation, $S_I/I^2 \approx A/f$,[32] or white noise, with the value of the Hooge parameter, $A \approx 5 \times 10^{-7}$, similar to those observed in unmodified pores of the same electrolyte

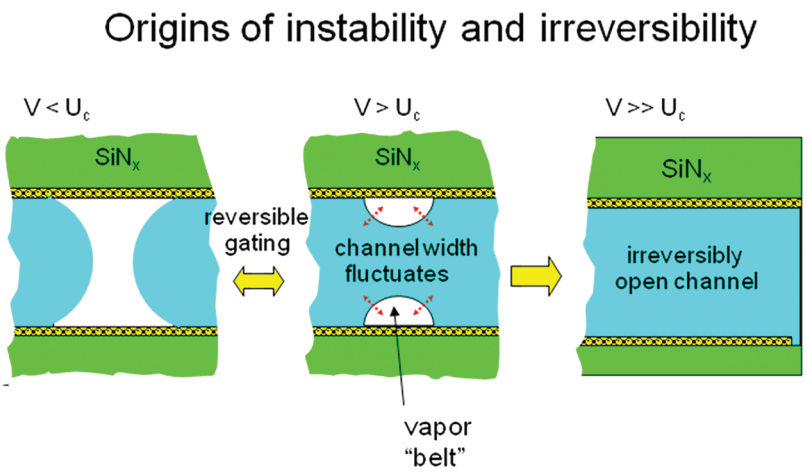

Figure 6. Illustration of water behavior inside a hydrophobic nanopore upon electrical shorting.

concentrations.[33] The noise near U_c (2.3 V in Figure 2B) formally also follows 1/*f* dependence but with 2 orders of magnitude larger $A \approx 5 \times 10^{-5}$. Moreover, the current has a distinct switching behavior between two states: with almost the same "low conductance" and more fluctuating "high conductance" states.

This accentuates the unique properties of hydrophobic nanopores compared with other ion conductive devices with nonlinear current–voltage characteristics. Hydrophobic nanopores have phase transition-like behavior between the dry and wet states for which the conductance change reflects the change in water occupation inside the pore. Transitions between these states can be gated by applied bias, which interrupts not only the ionic current but exchange of water and other solutes.

Molecular dynamics (MD) simulations on much smaller (D, H < 2 nm) hydrophobic nanopores[22–24] revealed the intermittent character of the hydrophobic nanopore wetting by water under equilibrium conditions. The duration of these stochastic periods of dry and wet states appeared to increase with the pore diameter, the dielectric constant of the membrane, and the electric field. These observations were qualitatively explained by a macroscopic description of competition between capillary and electrostatic contributions, in line with our conclusions. Because of the much smaller diameter and length, a comparatively minute activation barrier in the MD-modeled pores makes the time scale of stochastic pore wetting shorter, nanoseconds *vs* our seconds and minutes. For the same reason, there are no kinetically trapped wetted states in small pores and the wetting/dewetting phenomenon can be successfully analyzed based on thermodynamics. Yet, the expression for the critical bias of voltage-gated wetting, estimated using macroscopic thermodynamic considerations[23] and appearing very similar to our eq 5, was also found to exceed the results of MD simulations. Among the proposed explanations it was suggested that water restructuring could significantly change the surface tension near the hydrophobic surface, since MD simulations demonstrated that the water driven into the pore exhibits strong electrostrictive behavior. We see a similar behavior in the pores that are larger by 2 orders of magnitude, where the surface tension between water and the hydrophobic surface appears to be altered by electric field localized near the triple line because of nonzero surface conductance in a loosely packed self-assembled monolayer of hydrophobic molecules. Such an effect is not included in MD simulations, but its importance in small voltage-gated pores can probably be verified by explicit molecular representation of the hydrophobic walls, which would allow water molecules to penetrate into the hydrophobic layer.

CONCLUSIONS

We have demonstrated that short hydrophobically modified individual nanopores can be employed as voltage-gated ionic channels, where applied bias induces transitions between low-conductance dry state and high-conductance wet state. The conductance change of almost 3 orders of magnitude reflects not only the change in water occupation inside the pore but the ability for other solutes to move through the pore. The mechanism of operation is explained by electrowetting-induced change of the critical contact angle that allows movement of the menisci contact lines toward each other under electrostatic pressure from the applied bias. Transitions to the open wet state are irreversible for large-diameter pores but can be reversible for pores with diameters smaller than their length. The switching bias voltage, U_c, increases with the pore resistance in the closed state and with the surface hydrophobicity measured as a water contact angle on the corresponding flat surface. The reversibility depends upon the magnitude of the applied bias voltage, V, relative to U_c: For $V \geq U_c$, transitions are typically reversible, but if V is too large, $V \gg U_c$, a drop in the critical contact angle below 90° leaves no

bubble in the wetted state and prevents the pore from spontaneously drying when the bias is decreased. Nanopores with large U_c show more pronounced hysteresis in $I-V$ curves because of lower rates of induced wetting and drying. Hysteresis is less pronounced in nanopores with small U_c, but the two states can still be recognized in enhanced current fluctuations near U_c. These hydrophobic nanopores resemble voltage-gated biological channels despite being 2 orders of magnitude larger in size. It makes them good candidates for applications requiring efficient gating.

EXPERIMENTAL SECTION

Silicon nitride membranes were prepared by standard cleanroom processes as described previously.[34] In brief, 50 × 50 μm windows were defined by optical lithography on a 300 nm think LPCVD SiN ⟨100⟩ Si wafer with subsequent anisotropic KOH etching. Pore milling by focused ion beam was performed using an FEI dual-beam FIB instrument (10 pA, 30 kV ion current) with diameters from 60 to 600 nm (see Supporting Information).

Single-step silanization was done overnight from 2.5% solution of trimethoxyhexadecylsilane (SiH_{16}) in toluene with subsequent washing in pure toluene and baking at 120 °C for 1 h. Before the second modification, the membranes were wetted by ethanol and immersed in DI water for 30 min to hydrolyze unreacted methoxy groups and dried. A similar procedure was used for modification by the fluorosilane (heptadecafluoro-1,1,2,2-tetrahydrodecyl)trimethoxysilane (SiH_2F_8) with a 2.5% solution in toluene performed for 1 h with subsequent rinsing and baking.

The modification quality by silanes is sensitive to surface pretreatment, as it requires silanol groups that are very minimally present in native SiN. Pirahna treatment for 30 min was shown to be insufficient. The resulting surface hydrophobicity is significantly improved after 5 min oxygen plasma pretreatment (100 W) but exhibits a significant variability as measured by the contact angle with water on the flat portion of SiN film. The contact angles of such prepared surfaces were typically 95−100° (Supporting Information) but were further improved by repeating the modification step, which brought the contact angle close to 105°.

All measurements were performed in a custom-made electrochemical cell made from PDMS using degassed solutions of 1 M KCl in Tris buffer of pH 8 with Ag/AgCl electrodes placed within 5 mm on each side of the mounted membrane. The capacitance of the electrodes was maintained large enough to prevent any significant discharging during the course of an experiment even with an open pore with a large steady bias, which was verified by linear $I-V$ curves before and after the experiment. The cell was degassed (MaximaDry oil-free pump, Fisher) and then filled with the degassed electrolyte solution similar to the procedure described earlier.[13] The cell was equipped with windows allowing evaluation of the assembly under an optical microscope to ensure the absence of bubbles on the membrane surface, which were the major inconvenience for such hydrophobic membranes. A Keithley 6487 picoammeter was used to acquire all current−voltage data.

For the sake of simplicity, the value for a closed pore resistance (R_s) was defined as that at 0.5 V, and the critical bias voltage (U_c) as the voltage at which the current exceeds 5 nA. More than 40 devices were fabricated and tested. Some of them were prepared either with large diameters, which immediately became wet upon exposure to electrolyte, or modified with highly hydrophobic fluorosilane, which prevents electrolyte intrusion at biases < 20 V. The total number of devices that exhibited reversible switching between zero and finite conductance was 16.

Acknowledgment. I.V. is a Eugene P. Wigner Fellow at the Oak Ridge National Laboratory, managed by UT-Battelle, LLC, for the U.S. Department of Energy under Contract DE-AC05-00OR22725. This work was partially supported by a grant from the National Science Foundation (NSF DMR 0900238) to S.S. A portion of this research was conducted at the Center for Nanophase Materials Sciences, which is sponsored at Oak Ridge National Laboratory by the Office of Basic Energy Sciences, U.S. Department of Energy.

Supporting Information Available: Illustration of the setup, SEM images of nanopores, cell capacitance analysis, contact angle analysis, additional examples of $I-V$ curves through nanopores at different stages of surface modification with S_{16} and with SiH_2F_7, the analysis of the critical bias voltage correlation with pore diameter. This material is available free of charge via the Internet at http://pubs.acs.org.

REFERENCES AND NOTES

1. Kasianowicz, J.; Brandin, E.; Branton, D.; Deamer, D. Characterization of Individual Polynucleotide Molecules Using a Membrane Channel. *Proc. Natl. Acad. Sci. U. S. A.* **1996**, *93*, 13770–13773.
2. Li, J.; Gershow, M.; Stein, D.; Brandin, E.; Golovchenko, J. A. DNA Molecules and Configurations in a Solid-State Nanopore Microscope. *Nat. Mater.* **2003**, *2*, 611–615.
3. Bayley, H; Martin, C. R. Resistive-Pulse Sensing From Microbes to Molecules. *Chem. Rev.* **2000**, *100*, 2575–2594.
4. Vlassiouk, I.; Takmakov, P.; Smirnov, S. Sensing DNA Hybridization via Ionic Conductance through a Nanoporous Electrode. *Langmuir* **2005**, *21*, 4776–4778.
5. Vlassiouk, I.; Smirnov, S.; Siwy, Z. Ionic Selectivity of Single Nanochannels. *Nano Lett.* **2008**, *8*, 1978–1985.
6. Vlassiouk, I.; Siwy, Z. Nanofluidic Diode. *Nano Lett.* **2007**, *7*, 552–556.
7. Karnik, R.; Duan, C.; Castelino, K.; Daiguji, H.; Majumdar, A. Rectification of Ionic Current in a Nanofluidic Diode. *Nano Lett.* **2007**, *7*, 547–551.
8. Ali, M.; Ramirez, P.; Mafe, S.; Neumann, R.; Ensinger, W. A pH-Tunable Nanofluidic Diode with a Broad Range of Rectifying Properties. *ACS Nano* **2009**, *3*, 603–608.
9. Vlassiouk, I.; Smirnov, S.; Siwy, Z. Nanofluidic Ionic Diodes. Comparison of Analytical and Numerical Solutions. *ACS Nano* **2008**, *2*, 1589–1602.
10. Daiguji, H.; Oka, Y.; Shirono, K. Nanofluidic Diode and Bipolar Transistor. *Nano Lett.* **2005**, *5*, 2274–2280.
11. Vlassiouk, I.; Park, C.-D.; Vail, S. A.; Gust, D.; Smirnov, S. Control of Nanopore Wetting by a Photochromic Spiropyran: A Light-Controlled Valve and Electrical Switch. *Nano Lett.* **2006**, *6*, 1013–1017.
12. Smirnov, S.; Vlassiouk, I.; Rios, F.; Vail, S.; Gust, D. Electrical Conductance of Hydrophobic Membranes or What Happens Below the Surface. *Langmuir* **2007**, *23*, 7784–7792.
13. Smirnov, S.; Vlassiouk, I.; Takmakov, P.; Rios, F. Water Confinement in Hydrophobic Nanopores. Pressure Induced Wetting and Drying. *ACS Nano* **2010**, *4*, 5069–5075.
14. Rios, F.; Smirnov, S. pH Valve Based on Hydrophobicity Switching. *Chem. Mater.* **2011**, *16*, 3601–3605.
15. Rios, F.; Smirnov, S. Biochemically Responsive Smart Surface. *ACS Appl. Mater. Interfaces* **2009**, *1*, 768–774.
16. Lum, K.; Chandler, D. Phase Diagram and Free Energies of Vapor Films and Tubes for a Confined Fluid. *Int. J. Thermophys.* **1998**, *19*, 845–855.
17. Lum, K.; Luzar, A. Pathway to Surface-Induced Phase Transition of a Confined Fluid. *Phys. Rev. E* **1997**, *56*, R6283–R6286.
18. Luzar, A. Activation Barrier Scaling for Spontaneous Evaporation of Confined Water. *J. Phys. Chem. B* **2004**, *108*, 19859–19866.

19. Lefevre, B.; Saugey, A.; Barrat, J.-L.; Bocquet, L.; Charlaix, E.; Vigier, G.; Gobin, P.-F. Intrusion and Extrusion of Water in Hydrophobic Mesopores. *J. Chem. Phys.* **2004**, *120*, 4927–4938.
20. Husowitz, B.; Talanquer, V. Liquid−Vapor Oscillations of Water in Hydrophobic Nanopores. *J. Chem. Phys.* **2004**, *121*, 8021–8028.
21. Lee, C. Y.; McCammon, J. A.; Rossky, P. J. The Structure of Liquid Water at an Extended Hydrophobic Surface. *J. Chem. Phys.* **1984**, *80*, 4448–4455.
22. Allen, R. J.; Hansen, J.-P.; Melchionna, S. Molecular Dynamics Investigation of Water Permeation Through Nanopores. *J. Chem. Phys.* **2003**, *119*, 3905–3919.
23. Dzubiella, J.; Hansen, J.-P. Electric Field-Controlled Water and Ion Permeation of a Hydrophobic Nanopore. *J. Chem. Phys.* **2005**, *122*, 234706–14.
24. Beckstein, O.; Sansom, M. Liquid−Vapor Oscillations of Water in Hydrophobic Nanopores. *Proc. Natl. Acad. Sci. U. S. A.* **2003**, *100*, 7063–7068.
25. Jensen, M.; Borhani, D.; Lindorff-Larsen, K.; Maragakis, P.; Jogini, V.; Eastwood, M.; Dror, R.; Shaw, D. Principles of Conduction and Hydrophobic Gating in K^+ Channels. *Proc. Natl. Acad. Sci. U. S. A.* **2010**, *107*, 5833–5838.
26. Spronk, S.; Elmore, D.; Dougherty, D. Voltage-Dependent Hydration and Conduction Properties of the Hydrophobic Pore of the MscS Channel. *Biophys. J.* **2006**, *90*, 3555–3569.
27. Roth, R.; Gillespie, D.; Nonner, W.; Eisenberg, R. Bubbles, Gating, and Anesthetics in Ion Channels. *Biophys. J.* **2008**, *94*, 4282–4298.
28. Smith, D. P. H. The Electrohydrodynamic Atomization of Liquids. *IEEE Trans. Ind. Appl.* **1986**, *22*, 527–535.
29. Taylor, G. I. Disintegration of Water Drops in an Electric Field. *Proc. R. Soc. London A* **1964**, *280*, 383–397.
30. Hillebrandt, H.; Tanaka, M. Electrochemical Characterization of Self-Assembled Alkylsiloxane Monolayers on Indium-Tin Oxide (ITO) Semiconductor Electrodes. *J. Phys. Chem. B* **2001**, *105*, 4270–4276.
31. Chidsey, C. E. D.; Loiacono, D. N. Chemical Functionality in Self-Assembled Monolayers. Structural and Electrochemical Properties. *Langmuir* **1990**, *6*, 682–691.
32. Hooge, F. N.; Kleinpenning, T. G. M.; Vandamme, L. K. J. Experimental Studies on 1/f Noise. *Rep. Prog. Phys.* **1981**, *44*, 479–532.
33. Smeets, R. M. M.; Keyser, U. F.; Dekker, N. H.; Dekker, C. Noise in Solid-State Nanopores. *Proc. Natl. Acad. Sci. U. S. A.* **2008**, *105*, 417–421.
34. Vlassiouk, I.; Apel, P.; Dmitriev, S.; Healy, K.; Siwy, Z. Versatile Ultrathin Nanoporous Silicon Nitride Membranes. *Proc. Natl. Acad. Sci. U. S. A.* **2009**, *106*, 21039–21044.